Pressure-dependent Raman scattering of polycrystalline KNb$_{1-x}$Ta$_x$O$_3$ solid solutions

E. Di Geronimo[1] · V. Bornand[1] · Ph. Baranek[2] · Ph. Papet[1]

Abstract

We report experimental and calculated Raman scattering investigations of KNb$_{1-x}$Ta$_x$O$_3$ (x = 0.4, 0.5, 0.6) solid solutions as a function of hydrostatic pressure. The observed phase transitions sequence in the range from room pressure to 12 GPa is similar to the temperature-induced structural phase transformations: orthorhombic (ferroelectric) to tetragonal (ferroelectric) to cubic (paraelectric). Furthermore, it was observed that the domain of stability of ferroelectricity at high pressures increases with Nb-content. For the first time, some DFT calculations of theoretical Raman spectra are reported in order to support the experimental observations of pressure-induced phase transitions.

Keywords High pressure Raman spectroscopy · Phase transitions · Potassium niobate tantalite · DFT

1 Introduction

Over the last decade, lead-free ferroelectrics have gained major interest in functional materials research. Among the large family of ferroelectrics, the perovskite-type solid solution KNb$_{1-x}$Ta$_x$O$_3$ (KNT) appears as a potential alternative for lead-based ceramics in a wide range of electromechanical device applications, due to its good piezoelectric properties as well as environmental issues and human health [1–4]. Solid solutions of KNT exist as a single phase for the whole range of compositions, and all the phases crystallize in the perovskite structure but with different symmetries. Later studies have focused mainly on investigating the crystallographic and domain structures of these compounds. In an earlier work, Triebwasser established the composition-temperature phase diagram for KNbO$_3$-KTaO$_3$, pointing out a rhombohedral-orthorhombic-tetragonal-cubic phase sequence with increasing temperature [5]. Moreover, it has been reported that in KNT-based ceramics like (K, Na)(Ta, Nb)O$_3$ and (K,

Na, Li)(Ta, Nb, Sb)O$_3$ both the Curie temperature (T_C) and orthorhombic-tetragonal phase transition temperature (T_{O-T}) shifted to lower temperature as the concentration of Ta increases [6–9]. In addition, by using X-ray absorption Huan et al. showed the contribution of Ta displacements along different crystallographic orientations on (K, Na)NbO$_3$ ceramics, which tends to enhance the ferroelectric properties at the T_{O-T} [10]. Besides temperature variation, pressure change is another important variable providing complementary information about the different phase transitions that could be induced by pressure. Few reports deal with pressure-effect in the KNT system, which essentially concerns KNbO$_3$ and Nb-rich solid solutions of KNT. Gourdain et al. [11] and Kobayashi et al. [12] observed that the ferroelectric orthorhombic phase is stable up to 8–10 GPa and transforms to the paraelectric cubic phase through a weakly first-order transformation. Nevertheless, Shamim et al. [13] reported an orthorhombic to tetragonal phase transition around 7 GPa. Shamim et al. performed a high-pressure Raman study on KNT single crystals only

✉ V. Bornand, veronique.bornand@umontpellier.fr; E. Di Geronimo, edigerod@gmail.com; Ph. Baranek, philippe.baranek@edf.fr; Ph. Papet, philippe.papet@umontpellier.fr | [1]ICGM, Université Montpellier, CNRS, ENSCM, Montpellier, France. [2]EDF R&D, Department EFESE, EDF Lab Paris-Saclay, Palaiseau, France.

for Nb-rich solid solutions where an orthorhombic-tetragonal-cubic phase sequence was observed upon pressure with a limited domain of stability of the tetragonal structure [14].

In the present paper, high-pressure Raman spectroscopy experiments have been conducted on three polycrystalline samples, $KNb_{0.6}Ta_{0.4}O_3$ (KN60T40), $KNb_{0.5}Ta_{0.5}O_3$ (KN50T50) and $KNb_{0.4}Ta_{0.6}O_3$ (KN40T60) up to 12 GPa with the aim (1) to analyze the pressure-dependent phase transitions of these compounds and (2) to investigate the effect of Ta substitution on the possible sequences structural transitions of KNT polycrystalline samples with pressure. Besides, some DFT calculations of theoretical Raman spectra are reported in order to support the experimental observations of phase transition in the Raman spectra. This is the first time that such a theoretical versus experimental Raman study is conducted on KNT solid solutions.

2 Experimental procedure

$KNb_{1-x}Ta_xO_3$ (x = 0.4, 0.5, 0.6) powders were prepared by solid-state reaction of high purity K_2CO_3, Nb_2O_5 and Ta_2O_5 powders through a classical ceramic process. The starting raw materials were mixed stoichiometrically in ethanol and ground using an agate mortar and a pestle until a homogeneous dried mixture was obtained. In order to get a better reactivity, the mixed powders were uniaxial pressed and calcined at different temperature in a range 785 °C–1150 °C for 4 h. After the calcination, the samples were ground and mixed with alumina balls in an automatic planetary grinding machine (Fritsch Pulverisette 6) for 30 min at 400 rpm. The mixed powders were then sieved through a 100 μm. X-Ray Diffraction (XRD) using a PANAalytical X'pert pro diffractometer with Cu-Kα_1 radiation was used to identify the crystalline structure of the studied samples. The data were collected over 20° to 100° 2θ range with a 0.016 step size. Profile matching was performed with the use of the software FULLPROF [15]. Raman experiments were carried out with a Horiba LabRAM aramis Raman spectrometer using a 488 nm line of Ar$^+$ ion laser as the exciting source, which was focused on the surface of the sample by using an X 50 objective of a microscope. Data below ~125 cm^{-1} are artefacts due to the Rayleigh filter cut-off. Measurements were performed at room temperature both on increasing (up to 12 GPa) and decreasing pressure by using a membrane-type diamond anvil cell (DAC) with diamond culets of 500-μm diameter and a large angular access (50°) to collect the highest possible amount of scattered light. The sample was loaded along with a ruby sphere and a 4:1 methanol-ethanol mixture as the quasi-hydrostatic pressure-transmitting fluid into a chamber of 150 μm in diameter and

50 μm thick drilled in a stainless steel gasket. The DAC was closed by applying a pressure to the membrane, and the pressurization of the system was performed step-by-step using a homemade pressure controller equipped with a needle wire allowing a low helium flow rate to be delivered and a buffer system for low gas leak. The pressure was estimated based on the shift of the R_1 fluorescence line of the ruby [16, 17]. The Raman signal was obtained in the 100–1000 cm^{-1} range after a 10 min acquisition time. No intensity normalization has been done on all the recorded spectra reported in this paper.

3 Results and discussions

Figure 1 shows the room temperature XRD patterns collected for the three investigated compositions. We obtained highly crystallized materials without any detected second phases. In good agreement with published works, the Ta-rich $KNb_{0.4}Ta_{0.6}O_3$ (KN40T60) solid solution has a tetragonal symmetry while the Nb-rich $KNb_{0.6}Ta_{0.4}O_3$ (KN60T40) solid solution has an orthorhombic symmetry [5, 14, 18]. As already reported on KNT systems [5, 18], $KNb_{0.5}Ta_{0.5}O_3$ (KN50T50) is located at the limit between tetragonal and orthorhombic phases. However, in this work, best refinement could be obtained with an orthorhombic symmetry with this composition (Table 1). EDX analyses of each sample have confirmed the right stoichiometry of the powders, with no major compositional dispersion.

3.1 Hydrostatic pressure study

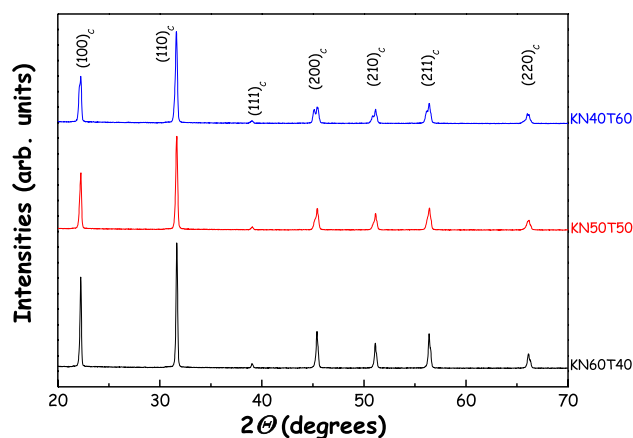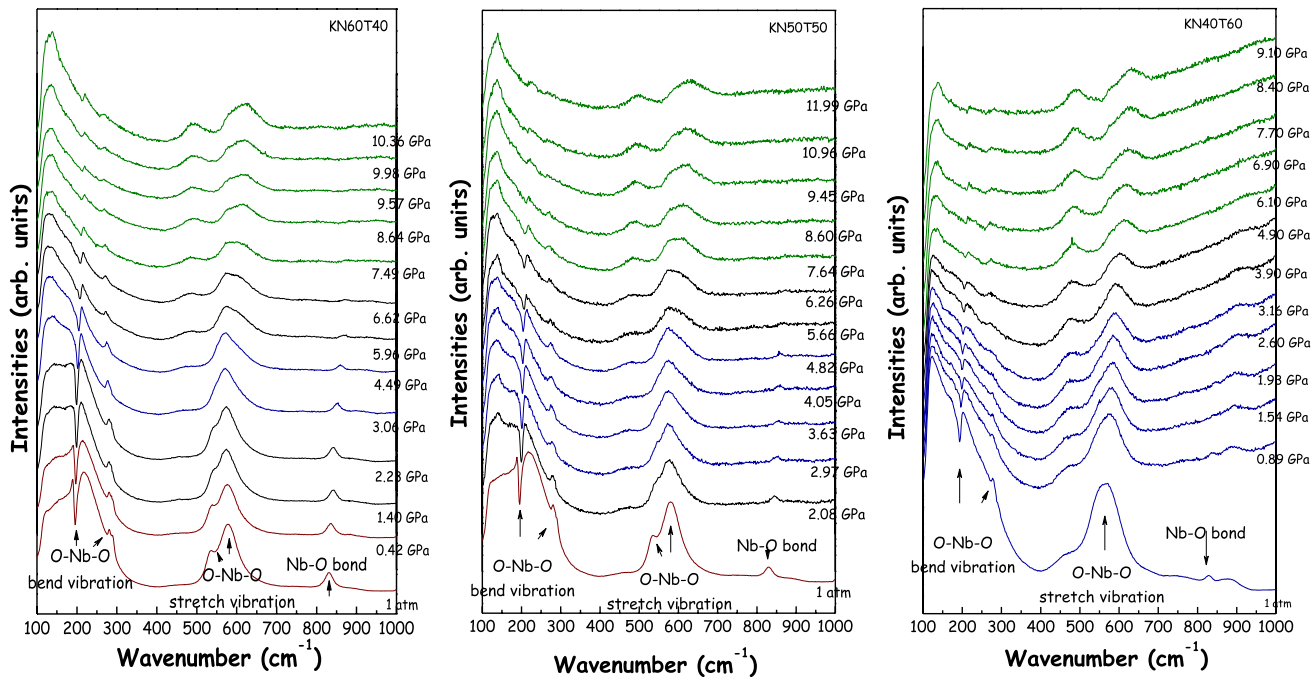Room temperature Raman spectra of the KNT samples with increasing pressure are shown in Fig. 2. We observe

Fig. 1 X-ray diffraction patterns of $KNb_{1-x}Ta_xO_3$ polycrystalline samples in the perovskite phase

Table 1 Details of lattice parameters and cell volume obtained from the XRD patterns through a Le Bail analysis compared with the ones obtained theoretically in this work

Composition	Space group		a (Å)	b (Å)	c (Å)	V (Å³)
$KNb_{0.4}Ta_{0.6}O_3$	P4mm	Exp.	3.993	3.993	4.002	63.808
		Calc.	3.985	3.985	4.076	64.727
$KNb_{0.5}Ta_{0.5}O_3$	Amm2	Exp.	3.992	5.649	5.702	64.292
		Calc.	3.982	5.680	5.692	64.370
$KNb_{0.6}Ta_{0.4}O_3$	Amm2	Exp.	3.991	5.655	5.689	64.198
		Calc.	3.982	5.663	5.674	63.974

Fig. 2 Raman spectra at room temperature of three different polycrystalline samples of $KNb_{1-x}Ta_xO_3$ as function of pressure. Colors are guide lines for the reader: brown spectra (orthorhombic phase), blue spectra (tetragonal phase), green spectra (cubic phase), black spectra (phase transition areas)

that the main features of the samples are modified as function of the pressure. This can give us a direct indication that structural phase transitions occurred in the materials within the investigated pressure range. Moreover, after releasing the high-pressure the powders recover their initial crystal structures, showing that changes are reversible without any relaxing or hysteresis phenomena.

Phase transitions in ABO_3-type alkali metal tantalates and niobates can be understood in terms of soft optical phonons, which may primarily involve either the vibrations or the rotations of the oxygen octahedral. The phase transitions are attributed to the condensation of these soft modes [19]. As it was shown in the reference [20, and other experimental and theoretical works cited in], these soft phonon are mainly IR-active and not Raman active (depending on the considered phase) and always involve a displacement and a deformation of the oxygen octadedra

while the roles of A and B cations vary among the materials and between high and low pressure phase transitions.

Raman studies on similar solid solutions of KNT depending on temperature have pointed out the main signatures of the different phase transitions induced by temperature, which are mainly dominated by bands related to the internal modes of the (Nb, Ta)O_6 octahedra [20–22].The modes around 840 cm^{-1}, 560 cm^{-1} and the resonance-depth at 200 cm^{-1} will be the main features in the analyses of pressure induced phase transitions for this investigation. These Raman active modes are associated to the (Nb, Ta)O_6 octahedra with O_h symmetry which correspond to the Nb-O bond, and the stretch and bend vibrations of the O-Nb-O modes.

With increasing pressures and according to the composition, a series of orthorhombic to tetragonal to cubic (Nb-rich solid solutions) or tetragonal to cubic (Ta-rich

solid solutions) phase transitions can be observed. Due to the nature of Nb and Ta cations, no pressure-induced electronic contribution, like overlapping of orbital, is expected to affect their high-pressure behavior. Therefore, the distorsion and compressibility of bonds can be assumed to be the driving force of the structural modification under compression. With increasing pressure, the solid solutions evolve towards higher constrained structures with higher symmetry.

A decrease in the resonance-depth at 200 cm^{-1} and the loss of the low-wavenumber wing of the 560 cm^{-1} mode due to a transformation of the $B_1(TO_3)$ and $B_2(TO_3)$ modes into $E(TO_3)$ are the main characteristics of an orthorhombic to tetragonal (O-T) phase transition [17, 18]. The spectral deconvolution for the 500–650 cm^{-1} region of KN60T40 and KN50T50 are shown in Fig. 3, which illustrates the possible identification of the orthorhombic-to-tetragonal phase transition in KN60T40 and KN50T50 through the shoulder around 530 cm^{-1} (followed by the * symbol). Specifically, it can be clearly seen how as the pressure increases the $B_1(TO_3)$ mode disappears while the $B_2(TO_3)$ modes transforms into the $E(TO_3)$ mode and the phase transition takes place. The phase transformations might occur around 3 to 4 GPa for both KN60T40 and KN50T50 samples.

Three criteria can be followed to identify the tetragonal to cubic (T-C) phase transition and its associated critical pressure range. With increasing wavenumbers, we can quote: (1) the fading of the resonance depth around 200 cm^{-1} until it almost vanishes [22], (2) the appearance of a mode around 450 cm^{-1} which is first-order Raman inactive and can be only observed in second-order scattering spectra in the cubic phase [20, 23], and (3) the disappearance of the first-order $A_1(LO_3)$ mode around 840 cm^{-1}

which is forbidden in the cubic phase [20]. Qualitatively, the three compositions investigated in this study have the same high-pressure Raman signatures suggesting similar high-pressure crystal symmetry. The high-pressure spectra obtained in our investigation are similar to those reported by Manlief et al. at high temperatures [20]. At Room temperature, this T-C transition is located around 7–8 GPa for KN60T40 and KN50T50, and decreases around 5–6 GPa for the KN40T60 sample. The persistence of broad spectral features, even though a general loss in intensity can be observed along with a strong increase of the background signal, is a direct evidence that the material is not strictly speaking cubic on a local level, a behavior which is very commonly observed in ferroelectrics due to local polar fluctuations and/or local composition changes [22, 24, 25]. Existence of first-order Raman scattering in *Pm3m* structure refers to as disorder-induced Raman scattering and can be assigned to nanopolar domains, initiated from the fluctuations of the Nb and Ta ions among its allowed positions, whose structure is locally different from the average one [26, 27].

The transition pressures for the studied compositions were assigned from the above analysis and reviewed in Fig. 4. High pressure Raman studies have been already performed for KN60T40 crystals by Shamim et al. [14]. The authors reported that the O-T and T-C phase transitions might be at around 3 and 4 GPa, respectively. However, in our work, concerning polycrystalline materials, while the phase sequence is maintained, the domain of stability of the tetragonal phase, and the ferroelectric region, seems to be larger. In addition, we can observe that as we increase the amount of tantalum the T-C transition pressure and the associated ferroelectric-paraelectric transition line decrease. This may be due to the atomic

Fig. 3 Raman spectra for KNb$_{1-x}$Ta$_x$O$_3$ (x = 0.4, 0.5) in the 500–650 cm^{-1} region for polycrystalline samples as a function of increasing pressure. The spectral deconvolution illustrates the possible identification of the pressure-induced phase transitions that occur in the materials depending on the composition (* follows the pressure-induced decrease of the B$_1$(3TO) mode characteristic of the orthorhombic phase)
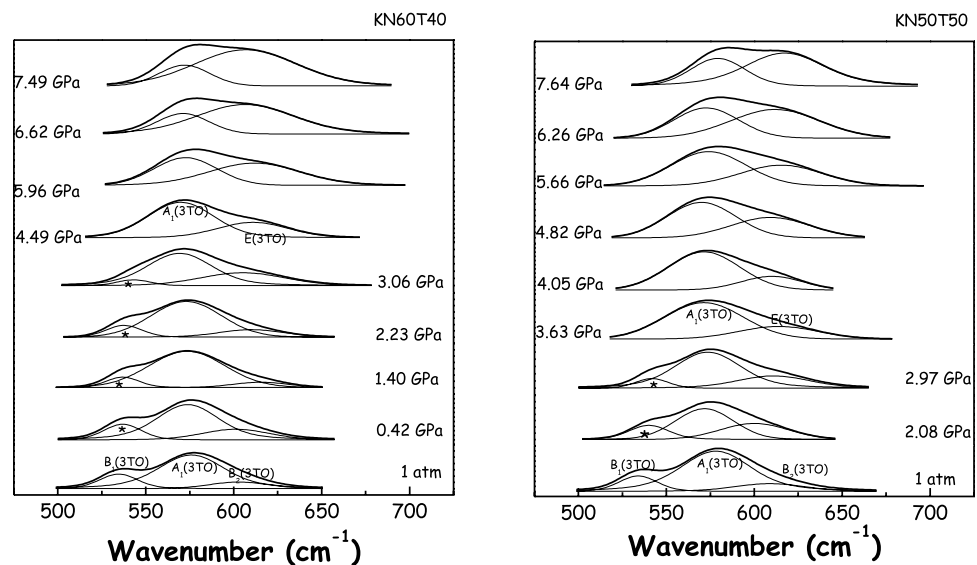
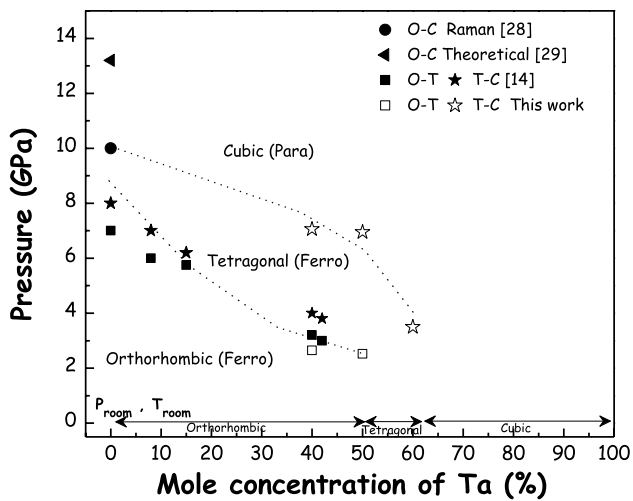**Fig. 4** Summary of the pressure-composition phase diagram for $KNb_{1-x}Ta_xO_3$ from this work and literature. Dash lines are guides to the eyes for the points of this work [14, 28, 29]

substitution that can cause a similar effect to the pressure [14], showing a connected chemical pressure and physical pressure effect.

3.2 Interpretation of Raman spectra: Insights from theory

3.2.1 Theoretical determination of the Raman spectra

The theoretical Raman spectra were calculated by using the Density Functional Theory (DFT) (at 0° K). The theoretical data were obtained with the periodic CRYSTAL14 [30, 31]. The used exchange—correlation functional is the hybrid PBE0 functional [32] which was shown to be the most adequate for the accurate description of the structural, electronic, vibrational and dielectric properties in agreement with experimental data for this family of materials [33]. Regarding the basis sets, an all—electron Gaussian type basis set was used for O; K, Nb and Ta were described with Gaussian type basis sets combined with pseudopotentials. A full description of these basis sets is given in reference [34]. As regards the computational conditions for the evaluation of the Coulomb and exchange series, the adopted thresholds on the overlap as defined in the CRYSTAL manual [31] are 10^{-8}, 10^{-8}, 10^{-8}, 10^{-8} and 10^{-16} a.u. Calculations were performed with a $8 \times 8 \times 8$ Monkhorst—Pack k-point mesh [35]. The Γ-point harmonic frequencies were calculated in the frozen phonons approximation.

The computed spectra were calculated considering ideal powders, with no preferred orientation, and assuming an incident light with a wavelength of 488 nm. They

were convoluted with a Gaussian equation with a damping factor of 8 cm^{-1}.

The different crystals have been simulated via a supercell approach. A $2 \times 2 \times 2$ supercell of the primitive K(Nb, Ta)O_3 have been used; for each "commensurate" concentration, all non-identical substitution patterns have been considered. For each of them, the lattice parameters and internal coordinates have been optimized, maintaining the cubic Pm-3m symmetry (10 configurations by concentration). For the configuration minimizing the total energy, the calculation of Γ phonons was performed in order to determine the unstable mode leading to the tetragonal or orthorhombic phases of $KNb_{1-x}Ta_xO_3$. For each concentration, the most stable configuration was retained and its equation of state was determined by fitting the calculated total energy E versus volume V curves by an integrated Murnaghan function. The volume V(P) is deduced from E(V). For each volume, E is minimized with respect to the crystallographic parameters: there are 8, 2 and 60 parameters to be optimized for the cubic, tetra and orthorhombic phases, respectively. Table 1 summarizes the obtained lattice parameters both theoretically and experimentally in this work: the average error between the theoretical and experimental results is about 0.5%. These simple models have been used to determine the different Raman spectra described in this paper.

3.2.2 Theoretical and experimental spectra

Figure 5 shows the experimental spectra compared with the computed ones at room pressure and room temperature for the different $KNb_{1-x}Ta_xO_3$ (x = 0.6, 0.5, 0.4) solid solutions. The calculations were performed in (1) a harmonic approximation and (2) at 0° K while the KTN system is (1) highly anharmonic and (2) the experiments were performed at room temperature. Besides, disorder in the system and possible local fluctuations in Nb and Ta ionic positions are responsible for the wide bands obtained in experiments while background substraction could not be done. Then a discrepancy between the experimental and theoretical calculations will arise.

The experimental and computed spectra at room temperature and different pressures (3 GPa, 7 GPa and 10 GPa) for the investigated solid solutions are displayed in Figs. 6, 7, and 8. For each pressure and each composition different spectra were calculated before being compared to experimental data. Discrepancies and/or shifts between calculated and observed spectra still subsist while the pressure is increased, attributed to the approximation required in the computation algorithm. However, comparison between theoretical values and available experimental ones are in a decent agreement specifically when the transition from the tetragonal
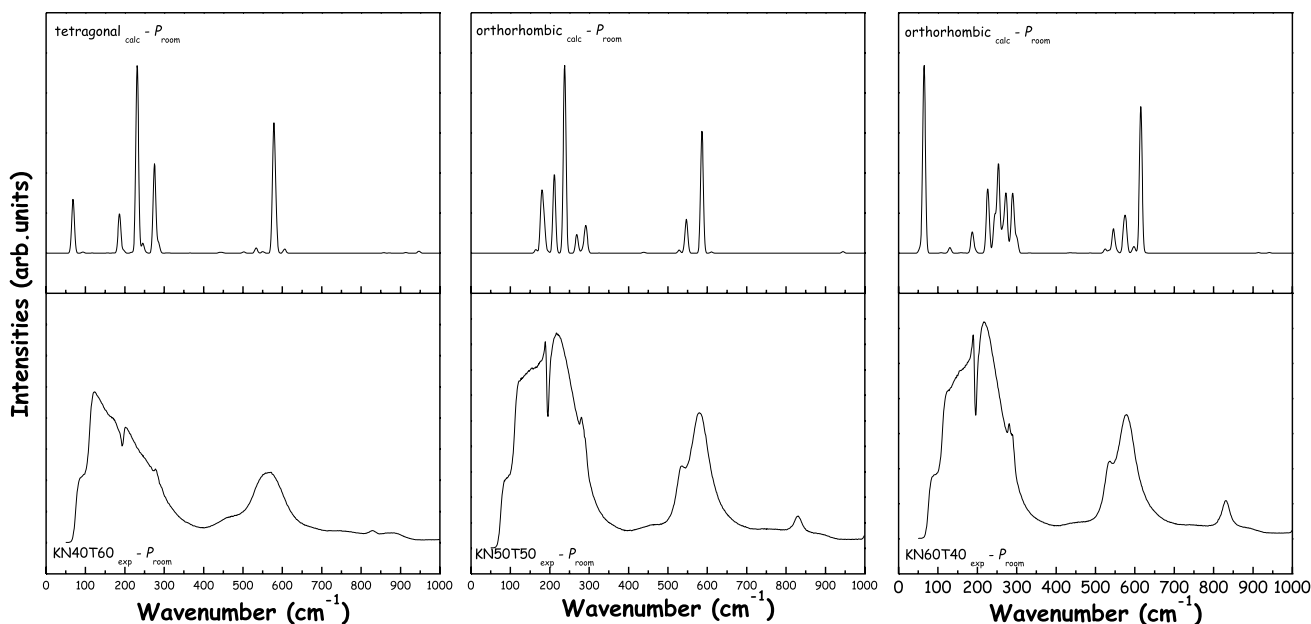
Fig. 5 Calculated (up) and experimental (down) Raman spectra for $KNb_{1-x}Ta_xO_3$ ($x = 0.6$, 0.5 and 0.4 from left to right) at room pressure
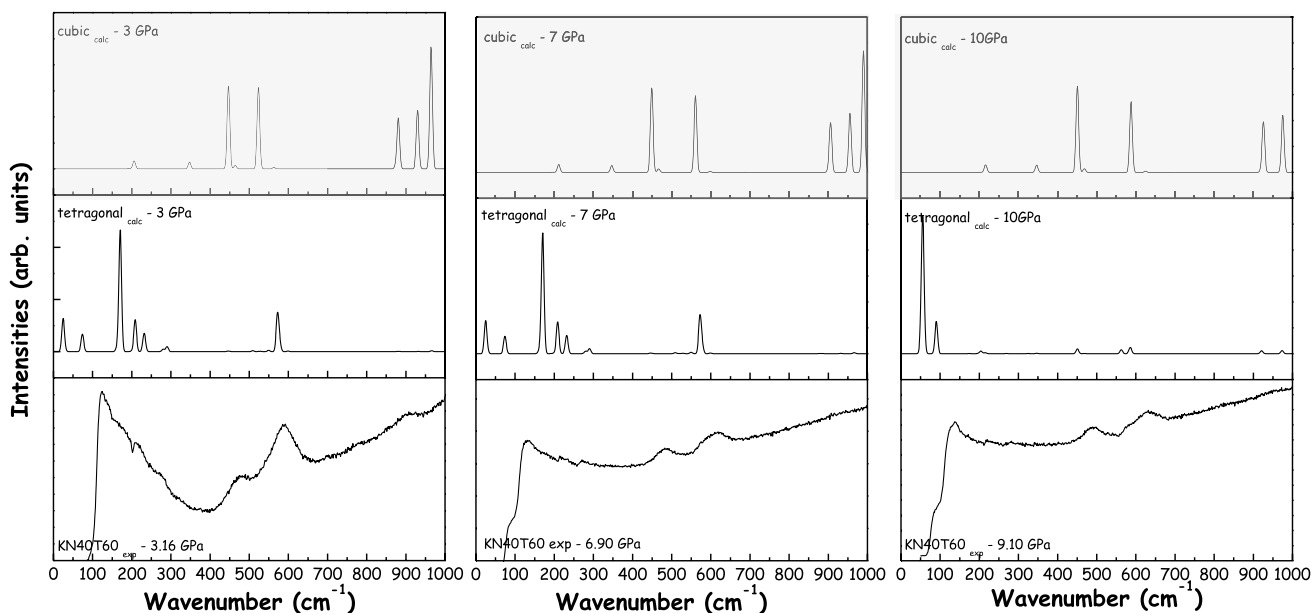

Fig. 6 Calculated and experimental Raman spectra for $KNb_{0.4}Ta_{0.6}O_3$ at 3 GPa, 7 GPa and 10 GPa (from left to right). For each pressure, theoretical spectra were calculated with tetragonal and cubic symmetries. Grey area corresponds to the best agreement between DFT calculations and theoretical datas

to the cubic phase takes place. Globally, DFT studies confirm (1) the pressure-induced phase-transition sequences observed for each system and (2) the pressure ranges in which phase transformations occur. The Ta-rich $KNb_{0.4}Ta_{0.6}O_3$ solid solution undergoes a tetragonal to cubic phase transition below 3 GPa. On the other side, the Nb-rich $KNb_{0.6}Ta_{0.4}O_3$ solid solution starts an orthorhombic to tetragonal phase transition around 3 GPa while the tetragonal to cubic phase transition is already complete at 7 GPa. The $KNb_{0.5}Ta_{0.5}O_3$ solid, located at the orthorhombic—tetragonal boundary at room pressure, begins a total orthorhombic to tetragonal transformation around 3 GPa while above 7 GPa the system is already cubic.
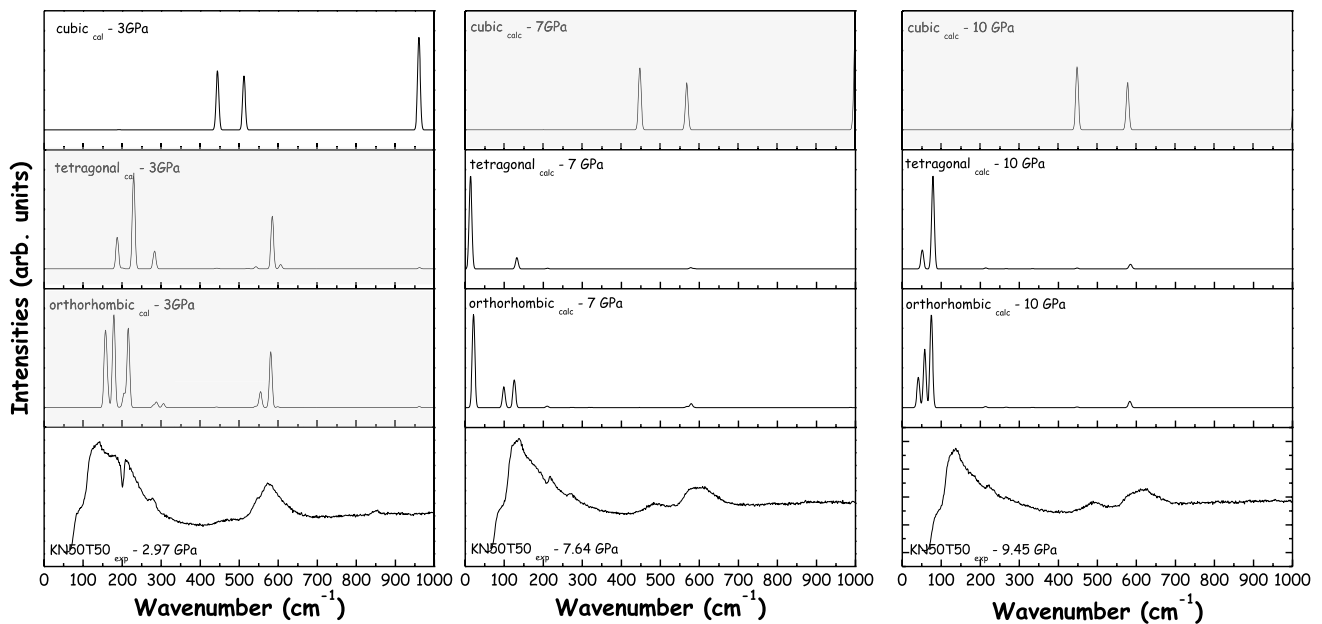
Fig. 7 Calculated and experimental Raman spectra for $KNb_{0.5}Ta_{0.5}O_3$ at 3 GPa, 7 GPa and 10 GPa (from left to right). Grey area: best agreement. For each pressure, theoretical spectra were calculated with orthorhombic, tetragonal and cubic symmetries. Grey area corresponds to the best agreement between DFT calculations and theoretical datas
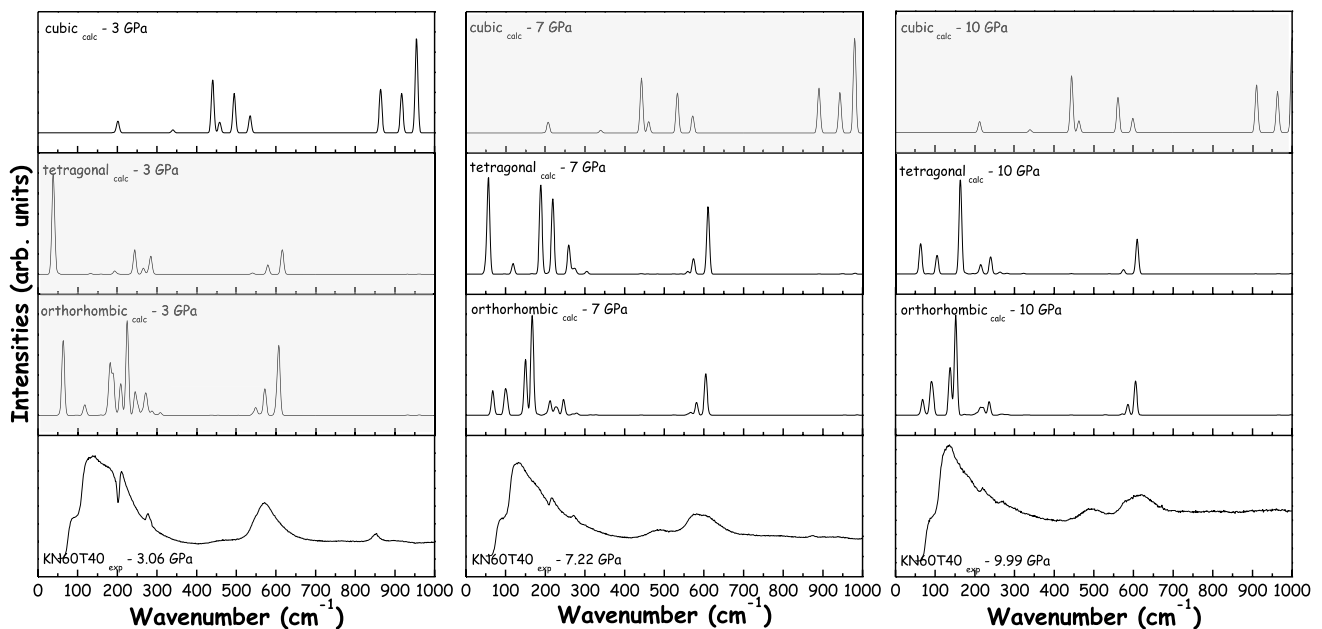

Fig. 8 Calculated and experimental Raman spectra for $KNb_{0.6}Ta_{0.4}O_3$ at 3 GPa, 7 GPa and 10 GPa (from left to right). For each pressure, theoretical spectra were calculated with orthorhombic, tetragonal and cubic symmetries. Grey area corresponds to the best agreement between DFT calculations and theoretical datas

4 Conclusion

We have conducted pressure-dependent Raman scattering experiments of $KNb_{1-x}Ta_xO_3$ (x = 0.4, 0.5, 0.6) polycrystalline samples, which provide evidence of pressure induce phase transitions. The phase transition sequences obtained in this work are similar to the temperature-dependent structural transformations reported in the literature. In addition, the tetragonal to cubic

phase transition occurs at higher pressures than the values reported for mixed crystals of the sample composition. This could suggest an enhancement of the ferroelectricity in polycrystalline solid solutions. Moreover, the domain of stability of ferroelectricity at high pressures decreases as the amount of tantalum increases.

Compliance with ethical standards

Conflict of interest The authors declare that they have no known competing financial interests or personal relationships that could have appeared to influence the work reported in this paper.

References

1. Cross LE (2004) Materials science—Lead-free at last. Nature 432:24–25
2. Rodel J, Klaus WJ, Seifert TP, Anton EM, Granzow T (2009) Perspective on the development of lead-free piezoceramics. J Am Ceram Soc 92:1153–1177
3. Eichel RA, Kungl H (2010) Recent developments and future perspectives of lead-free ferroelectrics. Funct Mat Lett 3:1–4
4. Panda PK, Sahoo S (2015) PZT to lead-free ceramics: a review. Ferroelectrics 474:128–143
5. Triebwasser S (1959) Study of ferroelectric transitions of solid solutions single crystals of $KNbO_3$-$KTaO_3$. Phys Rev 114:63–70
6. Schiemer J, Liu Y, Carpenter M, Withers R (2012) The effect of Ta doping on the phase transitions and the piezoelectric and ferroelectric properties of $K_{0.35}Na_{0.65}NbO_3$. Ferroelectrics 429:95–102
7. Lv Y, Wang C, Zhang J, Wu L, Zhao M, Xu J (2009) Tantalum influence on physical properties of $(K_{0.5}Na_{0.5})(Nb_{1-x}Ta_x)O_3$ ceramics. Mater Res Bull 44:284–287
8. Chang Y, Yang ZP, Ma D, Liu Z, Wang Z (2008) Phase transitional behavior, microstructure, and electrical properties in Ta-modified $[(K_{0.458}Na_{0.542})_{0.96}Li_{0.04}]NbO_3$ lead-free piezoelectric ceramics. J Appl Phys 104:024109
9. Yang Z, Chang Y, Wei L (2007) Phase transitional behavior and electrical properties of lead-free $(K_{0.44}Na_{0.52}Li_{0.04})(Nb_{0.96-x}Ta_xSb_{0.04})O_3$ piezoelectric ceramics. Appl Phys Lett 90:042911
10. Huan Y, Wang X, Li L (2014) Displacement of Ta-O bonds near polymorphic phase transition in Li-Ta-Sb-modified (K, Na)NbO_3 ceramics. Appl Phys Lett 104:242905
11. Gourdain D, Moya E, Chervin JC, Canny B, Pruzan P (1995) Ferroelectric-paraelectric phase transition in $KNbO_3$ at high pressure. Phys Rev B 52:3108–3112
12. Kobayashi Y, Endo S, Ashida T, Ming LC, Kikegawa T (2000) High-pressure phase above 40 GPa in ferroelectric $KNbO_3$. Phys Rev B 61:5819–5822
13. Shamim MM, Ishidate T (2000) Anomalous mode coupling and phase transition of $KNbO_3$ under high pressure. Solid State Comm 113:713–717
14. Shamim MM, Ishidate T, Ohi K (2003) High pressure Raman study of $KNbO_3$-$KTaO_3$ and $KNbO_3$-$NaNbO_3$ mixed crystals. J Phys Soc Jpn 72:551–555
15. Rodriguez-Carvajal J (2005) FullProf. https://www.ill.eu/sites/fullprof/php/downloads.html. Accessed 2008.
16. Mao H, Xu J, Bell P (1986) Calibration of the ruby pressure gauge to 800KBar under quasi-hydrostatic conditions. J Geophysical Res 91:4673–4676
17. Sherman WF, Wilkinson GR (1980) Raman and infrared studies of crystals at variable pressure and temperature. In: Clark RJH, Hester RE (eds) Advances in infrared and Raman spectroscopy. Heyden, London, pp 158–336
18. Rytz D, Scheel HJ (1982) Crystal growth of $KTa_{1-x}Nb_xO_3$ (0<x<0.04) solid solutions by a slow cooling method. J Cryst Growth 59:468–484
19. Fontana MD, Kugel GE, Vamvakas J, Carabatos C (1983) Persistence of tetragonal Raman lines in cubic $KNbO_3$. Solid State Comm 45:873–875
20. Manlief SK, Fan HY (1972) Raman spectrum of $KTa_{0.64}Nb_{0.36}O_3$. Phys Rev B 5:4046–4060
21. Zhang NN, Wei RS, Wang JY, Hu XB, Zhang HJ, Santos CC, Guedes I (2012) Phase transition investigation by Raman spectroscopy in highly diluted KTN crystals. J Alloys Compd 531:14–17
22. Bartasyte A, Kreisel J, Peng W, Guilloux-Viry M (2010) Temperature-dependent Raman scattering of $KTa_{1-x}Nb_xO_3$ thin films. Appl Phys Lett 96:262903
23. Rahaman MM, Imai T, Miyazu T, Kobayashi J, Tsukada S, Helal MA (2014) Relaxor-like dynamics of ferroelectric $K(Ta_{1-x}Nb_x)O_3$ crystals probed by inelastic light scattering. J Appl Phys 116:074110
24. Pruzan P, Gourdain D, Chervin JC (2007) Vibrational dynamics and phase diagram of $KNbO_3$ up to 30 GPa and from 20 to similar to 500 K. Phase Transit 80:1103–1130
25. Uwe H, Carter KB, Carter HL, Fleury PA (1986) Ferroelectric microregions and Raman scattering in $KTaO_3$. Phys Rev B 33:6436–6440
26. Sood AK, Chandrabbas N, Muthu DVS, Jayaraman A (1995) Phonon interference in $BaTiO_3$: High-pressure Raman study. Phys Rev B 51:8892–8896
27. Venkateswaran UD, Naik VM, Naik R (1998) High-pressure Raman studies of polycrystalline $BaTiO_3$. Phys Rev B 58:14256–14260
28. Shen Z, Hu ZP, Chong TC, Kuok MH (1995) Pressure-induced strong mode coupling and phase transitions in $KNbO_3$. Phys Rev B 52:3976–3980
29. Li S, Ahuja R, Johansson B (2002) Pressure-induced phase transitions of $KNbO_3$. J Phys Condens Matter 14:10873–10877
30. Dovesi R, Orlando R, Erba A, Zicovich-Wilson CM, Civalleri B, Casassa S, Maschio L, Ferrabone M, De La Pierre M, D'Arco P, Noel Y, Causa M, Rerat M, Kirtman B (2014) CRYSTAL14: a program for the Ab Initio investigation of crystalline solids. Int J Quantum Chem 114:1287–1317
31. Dovesi R, Saunders VR, Roetti C, Orlando R, Zicovich-Wilson CM, Pascale F, Civalleri B, Doll K, Harrison NM, Bush IJ, D'Arco P, Llunell M, Causà M, Noël Y (2014) CRYSTAL14 User's Manual. University of Torino, Torino
32. Adamo C, Barone V (1999) Toward reliable density functional methods without adjustable parameters: The PBE0 model. J Chem Phys 110:6158–6170
33. Sophia G, Baranek P, Sarrazin C, Rérat M, Dovesi R (2013) First-principles study of the mechanisms of the pressure-induced dielectric anomalies in ferroelectric perovskites. Phase Transiti 86:068–1084
34. Web site: http://www.crystal.unito.it/basis-sets.php
35. Monkhorst H, Pack J (1976) Special points for Brillouin zone integrations. Phys Rev B 13:5188–5192